Available online at www.sciencedirect.com

ScienceDirect

Geochimica et Cosmochimica Acta 226 (2018) 174–181

Geochimica et Cosmochimica Acta

www.elsevier.com/locate/gca

The impact of dissolved fluorine on bubble nucleation in hydrous rhyolite melts

James E. Gardner [a,*], Sahand Hajimirza [b], James D. Webster [c], Helge M. Gonnermann [b]

[a] Department of Geological Sciences, Jackson School of Geosciences, The University of Texas at Austin, Austin, TX 78712-0254, USA
[b] Department of Earth Sciences, Rice University, Houston, TX 77005, USA
[c] Department of Earth and Planetary Sciences, American Museum of Natural History, Central Park West at 79th, New York, NY 10024-5192, USA

Received 16 June 2017; accepted in revised form 3 February 2018; available online 13 February 2018

Abstract

Surface tension of hydrous rhyolitic melt is high enough that large degrees of supersaturation are needed to homogeneously nucleate H_2O bubbles during eruptive magma ascent. This study examines whether dissolved fluorine lowers surface tension of hydrous rhyolite, and thus lowers the supersaturation required for bubble nucleation. Fluorine was targeted because it, like H_2O, changes melt properties and is highly soluble, unlike all other common magmatic volatiles. Rhyolite melts were saturated at $P_s = 245$ MPa with H_2O fluid that contained F, generating rhyolite with 6.7 ± 0.4 wt.% H_2O and 1.1–1.3 wt.% F. When these melts were decompressed rapidly to $P_f = 149$–202 MPa and quenched after 60 s, bubbles nucleated at supersaturations of $\Delta P = P_s - P_f \geq 52$ MPa, and reached bubble number densities of $N_B = 10^{12–13}$ m^{-3} at $\Delta P = 78$–101 MPa. In comparison, rhyolite saturated with 6.34 ± 0.09 wt.% H_2O, but only 0.25 wt.% F, did not nucleate bubbles until $\Delta P \geq 100$–116 MPa, and even then, at significantly lower N_B ($<10^{10}$ m^{-3}). Numerical modeling of bubble nucleation and growth was used to estimate the values of surface tension required to generate the observed values of N_B. Slight differences in melt compositions (i.e., alkalinity and H_2O content), H_2O diffusivity, or melt viscosity cannot explain the observed differences in N_B. Instead, surface tension of F–rich rhyolite must be lower by approximately 4% than that of F–poor rhyolite. This difference in surface tension is significant and, for example, exceeds that found between hydrous basaltic andesite and hydrous rhyolite. These results suggest that is likely that surface tension for F–rich magmas, such as topaz rhyolite, is significantly lower than for F–poor magmas.

Keywords: Bubble; Nucleation; Rhyolite; Kinetics; Surface tension; H_2O; Fluorine

1. INTRODUCTION

Gas bubbles nucleate in magma when volatiles become supersaturated in the silicate melt (Sparks, 1978). In volcanic eruptions, volatile supersaturation ($\Delta P = P_s - P$) occurs when pressure on the magma (P) drops below the saturation pressure (P_s) of the volatile-bearing magma. The rate at which bubbles nucleate depends critically on the surface energy required to create clusters of molecules, called nuclei, of sufficient size to grow into bubbles. Surface energy, in turn, depends on the surface tension between a bubble and its surrounding medium. In the absence of solid substrates that can act as sites for nucleation, bubble nucleation will be homogeneous and nucleation rate will depend, in addition to ΔP, on surface tension. All else being equal, a

* Corresponding author. Fax: +1 512 471 9425.
E-mail address: gardner@mail.utexas.edu (J.E. Gardner).

https://doi.org/10.1016/j.gca.2018.02.013
0016-7037/

small decrease in surface tension lowers the surface energy of a bubble nucleus and, consequently, produces a substantial increase in bubble nucleation rate (e.g., Hurwitz and Navon, 1994).

Experimentally, it has been found that H_2O bubbles nucleate homogeneously in rhyolite melt only when ΔP exceeds about 100–125 MPa (Mourtada-Bonnefoi and Laporte, 1999; Gardner and Webster, 2016). At $\Delta P \approx$ 100–125 MPa, the induction time (Kashchiev, 2000; Gonnermann and Gardner, 2013), which is the statistically averaged time required to nucleate a bubble within a given volume of melt, is longer than the typical duration of 10's to a few 100's of seconds for decompression experiments. At higher values than this critical ΔP, the induction time becomes shorter than experimental time and thus the number of bubbles that nucleate during an experiment increases with ΔP. Rhyolite melts that contain less than ~4 wt.% H_2O, therefore, do not nucleate bubbles experimentally (Mourtada-Bonnefoi and Laporte, 1999; Gardner and Webster, 2016), because $P_s \leq$ 100–125 MPa (c.f., Liu et al., 2005). It has also been found that the addition of CO_2 to H_2O-rich rhyolite does not appreciably change the induction time for bubble nucleation in rhyolite with ~4 wt.% H_2O (Mourtada-Bonnefoi and Laporte, 1999; Gardner and Webster, 2016).

The objective of this study is to examine whether the addition of fluorine (F) will significantly affect the number of bubbles nucleated in H_2O-rich rhyolite at a given value of ΔP, all else being equal. We examine F in rhyolite because, unlike all other volatiles other than H_2O, it is highly soluble, and lowers melt viscosity and the liquidus temperature (Manning, 1981; Dingwell et al., 1985; Carroll and Webster, 1994; Giordano et al., 2004; Mysen et al., 2004; Kiprianov, 2006; Webster and Thomas, 2006; Dolejš and Baker, 2007; Zimova and Webb, 2007; Baasner et al., 2013). Thus, our objective is to assess whether dissolved F affects surface tension, as does H_2O (Gardner et al., 2013). To this end we performed a series of decompression experiments using H_2O-saturated rhyolite as a control group and compare them to a second series of decompressions that are chemically very similar, other than subtle differences in Na, Fe, and H_2O contents, except for higher concentrations of dissolved F.

2. EXPERIMENTAL MATERIALS AND METHODS

All experiments used cylinders cored from a metaluminous, high-silica rhyolitic obsidian that has been used in other nucleation studies (Gardner, 2009; Gardner and Ketcham, 2011; Gardner et al., 2013; Gardner and Webster, 2016). Most cylinders were 11–13 mm long and 2.7 mm in diameter. Three cylinders and enough distilled water to ensure that the samples were fluid saturated were sealed inside Au capsules, and each capsule was placed into externally heated, cold-seal pressure vessels and run at 850 °C (±5 °C) and 250 MPa (±0.1 MPa) for ~7 days (Table 1). Two other cylinders with distilled water (again, enough to ensure fluid saturation) and NaF were added to Pt capsules, and each was placed into an internally heated pressure vessel (IHPV) and run at ~1100 °C and 245 MPa for ~7 days. After each experiment, the capsule was checked that no weight was lost. When each capsule was cracked open, a separate fluid was found in each one, showing that all runs were fluid saturated. Samples were then extracted from their capsules, and sectioned into smaller samples using a slow speed saw. Each was ~0.5 cm long and weighed ≥50 mg. A thin wafer (~1 mm thick) was also sliced from the center of each sample and used to analyze volatile contents and melt composition (see below).

Each sample used in a decompression experiment was loaded into an Au capsule, which was welded shut and placed into a cup on the end of an Inconel rod that was then inserted into a rapid-quench, cold-seal pressure vessel. The sample was held in the water-cooled region of the vessel while the pressure vessel was heated to 850 °C (Table 2). The Inconel rod was then raised with an external magnet to insert the sample into the hot zone of the pressure vessel. Pressure was quickly adjusted to 251 MPa, slightly above saturation pressure to suppress any exsolution, using a hand-operated intensifier. After a sample was heated for 5 min, pressure was released quickly to a lower final pressure (P_f), by opening the pressure vessel to a large pressure reservoir that had been set at some low pressure. This caused very rapid drops in pressure that can be timed precisely ($\leq 2.5 \pm 0.1$ s). The sample was then held at P_f before being rapidly quenched by lowering it back into the water-cooled jacket. The total time that all samples spent below P_s was 60 s (Table 2). When the sample was lowered, cool water replaced it in the hot zone, which heats, resulting in a near-instantaneous pressure increase. For all decompressions, pressure increased 5–6 MPa.

All samples were examined to see whether bubbles nucleated (Fig. 1). If they had, their sizes and number density (N_B; in numbers m^{-3}) were measured using a petrographic microscope. N_B was measured by selecting 4–5 areas (40 μm × 40 μm) in a sample and counting all bubbles that appear as the field of view is moved through it using the focusing knob of the microscope. The thickness of each volume measured, typically 800–2000 μm, was recorded by a Heidenhain focus drive linear encoder that detects the motion of the stage, and is precise to ±0.6 μm. The typical volume analyzed was ~0.01 cm^3, and so the detection limit on N_B is ~10^8 m^{-3}.

Dissolved H_2O contents were analyzed with a ThermoElectron Nicolet 6700 spectrometer and Continuμm IR microscope. Concentrations of molecular (H_2O_m) and hydroxl (OH^-) H_2O were determined from absorbances at ~5250 and ~4500 cm^{-1}, using white light and a CaF_2 beamsplitter and the model of Zhang et al. (1997). Reported H_2O contents are the averaged sums of H_2O_m and OH^- (Table 2). Sample thicknesses were measured with the focus drive encoder described above.

Concentrations of major elements and F were measured in starting and run-product glasses using a JEOL JXA-8200 electron probe micro-analyzer (EPMA) and Probe For EPMA software (Donovan, 1995) at the University of Texas at Austin. Six analyses were measured per sample, using a 15-kV and 10-nA beam with a 10-μm diameter. A mean atomic number background correction was used for all analyses. Fluorine was measured using 90 s count times,

Table 1
Samples used in decompression experiments.[a]

	G–1590	*G–1591*	*G–1680*	*F–02*	*F–03*
SiO_2	76.64	–	–	75.02	75.22
TiO_2	0.02	–	–	0.05	0.04
Al_2O_3	13.01	–	–	12.82	12.56
FeO*	0.80	–	–	0.36	0.46
MnO	0.04	–	–	0.05	0.06
MgO	0.01	–	–	0.02	0.08
CaO	0.70	–	–	0.57	0.72
Na_2O	4.02	–	–	6.31	6.06
K_2O	4.75	–	–	4.79	4.78
H_2O	6.29 ± 0.01	6.29 ± 0.02	6.45 ± 0.08	6.99 ± 0.25	6.39 ± 0.06
F	0.25 ± 0.02	–	–	1.34 ± 0.30	1.10 ± 0.18
A/CNK	1.0	–	–	0.77	0.76
N/NK	0.56	–	–	0.67	0.66

[a] G–1590, G–1591, and G–1680 are obsidian cores that were hydrated; F–02 and F–03 are obsidian cores that were hydrated and fluorinated. Major elements (normalized to 100%) and F measured by electron microprobe, with all Fe reported as FeO; oxides are in wt.%; H_2O measured by FTIR. Concentrations of H_2O and F are listed in wt.% with ±1 s errors. "–" = not analyzed.

Table 2
Decompression experiments: Conditions and results.[a]

Run	Starting Material	P_i (MPa)	P_f (MPa)	T (°C)	Time	F (wt.%)	log N_B (m^{-3})	d (μm)	σ (N m^{-1})
G–1621	F–03	251	222.5	850	1.0/59.0	–	0	–	–
G–1630	F–03	251	202.0	850	1.9/58.1	0.93 ± 0.06	0	–	–
G–1618	F–02	251	197.5	850	1.6/58.4	1.21 ± 0.16	9.8	11 ± 1	0.037
G–1615	F–02	251	172.5	850	2.0/58.0	–	11.8	21 ± 4	0.047
G–1629	F–03	251	149.5	850	2.0/58.0	1.27 ± 0.18	13.0	8 ± 3	0.055
G–1613	F–02	251	149.0	850	2.0/58.0	1.13 ± 0.08	11.9	22 ± 8	0.056
G–1636	G–1590	251	200.0	850	1.4/58.6	–	0	–	–
G–1639	G–1591	251	180.0	850	1.8/58.2	–	0	–	–
G–1611	G–1590	251	173.5	850	2.0/58.0	–	0	–	–
G–1609	G–1590	251	149.0	850	2.4/57.6	–	9.4	54 ± 11	0.058
G–1645	G–1591	251	149.0	850	1.9/58.1	–	0	–	–
G–1685	G–1680	251	134.0	850	1.7/58.3	–	9.3	57 ± 2	0.065

[a] Compositions of starting materials are listed in Table 1. P_i and P_f = initial and final pressures of the experiment. Times are number of seconds it took to lower pressure to P_f (±1 s)/number of seconds held at P_f. F (in wt.%) dissolved in glasses measured by electron microprobe (±2 s errors). N_B is the number density of bubbles nucleated, and d is the average diameter of bubbles nucleated. "–" = not analyzed. The estimated surface tension (s) to produce the observed N_B for the given decompression is given for experiments that nucleated bubbles; errors on σ are $\leq$0.001 N m^{-1}.

with a larger (3-mm) slit size to improve counts. All other elements (Na, Mg, Al, Si, K, Ca, Mn, Fe, Ti) were measured using 20 s count times and a standard (0.3-mm) slit size. A secondary glass standard was measured periodically to ensure accuracy of the data.

3. EXPERIMENTAL RESULTS

Melt compositions of the starting materials differ slightly, depending on the method used (Table 1). The dissociation of NaF as the source of F enriched the melt in Na_2O, which changed their alkalinity relative to those that were only hydrated, as measured by the molar ratios A/CNK [$=Al_2O_3/(CaO + Na_2O + K_2O)$] and N/NK [$=Na_2O/(Na_2O + K_2O)$]. It also appears that some FeO was lost from the melt to the Pt tubing. Within error, most others elements were present in all glasses at the same concentrations.

Starting materials were generated in the presence of a separate fluid of H_2O or H_2O+F, and hence all were fluid saturated. The glasses of the three samples hydrated without added NaF contain ~0.25 wt.% F and, on average, 6.34 ± 0.09 wt.% H_2O (Table 1). This H_2O content agrees within error of that predicted by the solubility model of Liu et al. (2005). The samples hydrated and fluorinated at 1100 °C and 245 MPa contain 1.1–1.4 wt.% F. At those conditions, the model of Liu et al. predicts that H_2O solubility is ~0.4 wt.% lower than at 850 °C and 250 MPa. On the other hand, the data presented by Holtz et al. (1993) argues that adding ~1.0 wt.% F to the melt increases H_2O solubility by ~0.4 wt.%. Overall, therefore, samples F–02 and F–03 should have equal or slightly higher H_2O

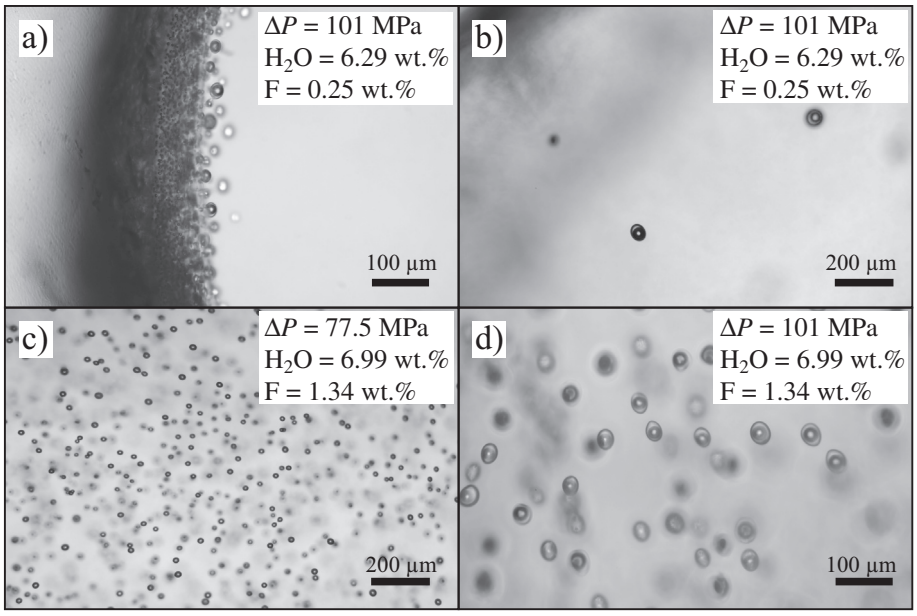

Fig. 1. Photomicrographs of representative experiments (scale bars shown in each): (a) G–1609, showing fringe bubbles that nucleated heterogeneously along the edge of the sample; (b) G–1609, showing isolated bubbles that homogeneously nucleated in F–poor rhyolite melt; (c) G–1615 and (d) G–1613, showing bubbles that nucleated in the interiors of F–rich rhyolite melts. Note the many more bubbles in (d) compared to (b), both of which decompressed to the same final pressure.

contents than those hydrated only, and indeed they contain, on average, 6.7 ± 0.4 wt.% H_2O (Table 1).

In the decompression experiments, numerous bubbles (often < 10 μm) grew in the outer fringes of all samples (Fig. 1a). Such "fringe" bubbles occur almost invariably in decompressions of hydrous melts, and result from heterogeneous nucleation at the contact with the metal capsule (Mangan and Sisson, 2000). We ignore these bubbles, and instead focus on the interiors of samples, because we are interested in the conditions needed to nucleate bubbles homogeneously in rhyolite melt (Fig. 1b). This is justified, because the characteristic diffusion length scale during the experiments is at least one order of magnitude shorter than the distance between capsule wall and sample interior.

Decompressions of hydrated rhyolites that contain ~0.25 wt.% F establish reference conditions (Table 2). Bubbles nucleated in these melts only when decompressed to P_f = 134–149 MPa, and thus at ΔP = 101–116 MPa (Fig. 2). Similar numbers of bubbles nucleated at these pressures, and were ~55 μm in diameter (Fig. 1b). The absence of bubbles in sample G–1645 (P_f = 149 MPa) and low N_B values in samples G–1609 and G–1685 suggest that ΔP = 101–116 MPa was not high enough for the induction time to become significantly shorter than the experimental duration.

Hydrous rhyolites with 1.1–1.4 wt.% F were decompressed to P_f = 149–222.5 MPa (Table 2). Four run-product glasses, three of which nucleated bubbles, were analyzed for their F contents and found to contain concentrations within error of the initial values. No bubbles nucleated at P_f = 202 MPa, whereas bubbles nucleated in all samples decompressed to P_f <198 MPa. For these melts, therefore, the induction time becomes less than the experimental time scale when ΔP exceeds ~ 48 MPa (Fig. 2). At ΔP = 77.5, $N_B \approx 10^{12}$ m^{-3}, and at ΔP = 100 MPa, N_B reached 10^{13} m^{-3} (Fig. 1c and d). Importantly, at similar values of ΔP, samples with 1.1–1.4 wt.% F

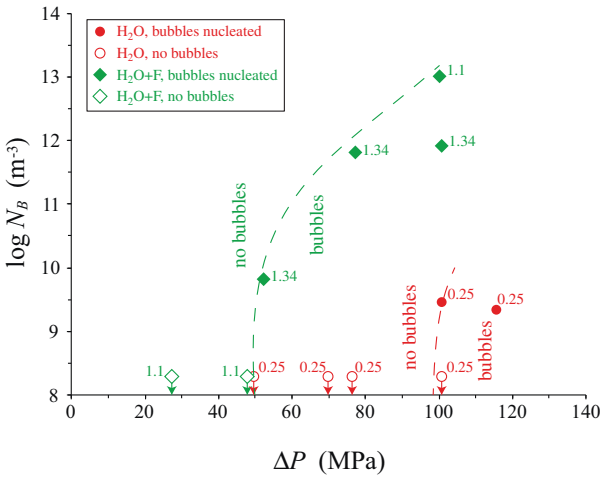

Fig. 2. Variations in bubble number density (N_B; bubbles per m^3) as a function of supersaturation (ΔP). Green diamonds are samples with 1.1–1.3 wt.% F; red circles are those with 0.25 wt.% F (F contents are listed next to each symbol for reference). Open symbols with arrows are samples that did not nucleate bubbles (N_B = 0). The approximate detection limit on bubble number density, based on the typical volume of sample measured, is 10^8 m^{-3}. The dashed curves divide conditions at which bubbles nucleate versus conditions that do not generate bubbles. (For interpretation of the references to colour in this figure legend, the reader is referred to the web version of this article.)

nucleated orders of magnitude more bubbles than those with 0.25 wt.% F. The bubbles in the F–rich samples are substantially smaller than those in F–poor samples, in accord with the orders of magnitude increases in N_B (Gardner et al., 1999).

4. ESTIMATION OF NUCLEATION RATE AND SURFACE TENSION

To augment the quantitative evaluation of our experimental results we modeled bubble nucleation and growth during decompression of the experimental samples. The numerical model is described in sufficient detail by Toramaru (1995). We integrate the coupled ordinary differential equations for nucleation rate for bubble number density, as well as conservation of mass and momentum for bubble growth, using the MATLAB ordinary differential equation solver *ode15s*. In contrast to Toramaru (1995), however, we used the empirical formulation for water diffusivity (D_{H_2O}) of Zhang and Behrens (2000), as well as the melt viscosity models of Giordano et al. (2008). Furthermore, we used the H_2O solubility model of Liu et al. (2005), adjusted for the slight increase expected as a result of added F, based on the experiments by Holtz et al. (1993).

For each experiment, we estimated the value of surface tension at which the model correctly predicts the observed N_B, assuming that surface tension is constant throughout the given experiment (Fig. 3). For those experiments where no bubbles nucleated within the sample interior we estimated the value of surface tension at which a bubble would be predicted to nucleate within the sample, which in principle corresponds to conditions where the induction time equals the time of the experiment. It should be noted that surface tension in those samples is probably higher than this minimum estimate.

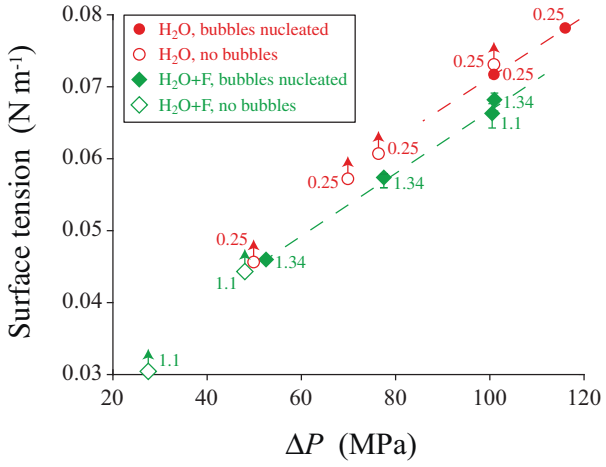

Fig. 3. Estimated surface tension as a function of supersaturation pressure (ΔP). Symbols are the same as those in Fig. 2. Error bars (when greater than symbol size) cover the range of possible values of surface tension, assuming an order of magnitude change in H_2O diffusivity. Dashed curves connect samples that nucleated bubbles. Note that reported surface tension estimates for samples that did not nucleate bubbles are minimum values.

5. DISCUSSION

5.1. Retention or resorption of bubbles during experimental quench

After decompression and during the quench of the samples, pressure is observed to rise by 5–6 MPa as described previously. Recently, McIntosh et al. (2014) found halos of glass enriched in H_2O around quenched bubbles in such experiments. They interpret such halos as recording resorption of H_2O back into the melt during cooling, and suggest that bubbles can partly resorb into the melt. Resorption occurs mainly because the solubility of H_2O increases as temperature decreases at pressures below ca. 400 MPa (Holtz et al., 1995) One could thus argue that the absence of bubbles in some decompressed samples is an artifact resulting from complete resorption of bubbles (with the microscope used we can identify bubbles as small as 0.5 μm in size). Two observations allow us to reject this argument. First, the same amount of resorption should occur in samples that undergo similar amounts of decompression and rate of quenching. All experiments in this study experienced similar amounts of pressure drop and the same rates of quenching (Table 2). Bubbles exist in hydrous rhyolite melts with 1.1–1.4 wt.% F at $P_f = 149$–202 MPa. In contrast, hydrous rhyolite melts with ~0.25 wt.% F contain no bubbles at $P_f > 149$ MPa. It is not tenable to suggest that bubbles had nucleated in the F–poor melts at higher pressures, only to have them all resorb completely during the quench, when the relatively F–rich melts still contain visible bubbles at pressures as high 202 MPa. Second, as previously mentioned, fringe bubbles nucleate along the melt–capsule contact during decompressions (Fig. 1a). Those bubbles are seen in all decompressions, including those that lack bubbles in the interiors (Fig. 1a). Again, it is not tenable to suggest that the absence of interior bubbles is an artefact of complete resorption when fringe bubbles did not resorb.

To examine this further, we modeled H_2O resorption from 1 μm bubbles. The modeling accounted for the rate of change in temperature during sample quenching, which equals ~150 °C s^{-1} (Dobsan et al., 1990), and the corresponding increase in solubility (following the model of Liu et al., 2005) and decrease in diffusivity (Zhang and Behrens, 2000). We find that during quenching there could be at most a decrease on the order of 10% in mass and radius. Hence, even bubbles that were originally 1 μm in size would still be observable in our samples. The absence of bubbles in the F–rich melts at relatively high pressures thus cannot be the result of resorption during sample quench.

5.2. Controls of experimental parameters on bubble nucleation

All melts were decompressed to overlapping values of P_f, the time taken to drop to P_f was the same, and all were held at P_f for the same amount of time (Table 2). Hence, the marked difference in N_B cannot be explained by decompression conditions. There are subtle differences in melt

alkalinity, which arose from the methods used to create the starting materials (Table 1). It should be noted that large differences in melt composition (basaltic andesite to rhyolite) have been found to have little impact on bubble nucleation (Gardner et al., 2013). In this study, the Na_2O contents of the melts differ by ~2–2.3 wt.% (Table 1), because F was added through dissolution of NaF. The addition of Na can affect surface tension of silicate melts, which in turn would impact the kinetics of bubble nucleation, with a decrease in surface tension promoting nucleation (Hurwitz and Navon, 1994; Gonnermann and Gardner, 2013). The impact of Na_2O on surface tension, however, differs for different melt compositions. In the system Na_2O–SiO_2, increasing the amount of Na_2O increases surface tension at any given temperature (Shartsis and Spinner, 1951). At 1000 °C, for example, surface tension is higher by 0.077 N m^{-1} with the addition of 10 wt.% Na_2O, from 20 to 30 wt.%. The impact of Na_2O is similar at lower temperatures, with the addition of 2.8 wt.% Na_2O (30.8–33.6) increasing surface tension by 0.003 N m^{-1} at 900 °C. In contrast, in haplogranitic melts an increase in Na_2O from 4.6 to 9.0 wt.% reduces surface tension by 0.010–0.016 N m^{-1} at temperatures above 1000 °C (Bagdassarov et al., 2000). Unfortunately, surface tension of relatively Na–poor haplogranitic melt was not measured at colder temperatures, but variations in surface tension with temperature for the two melts suggest that surface tension decreases more for the Na–poor melt than for the Na–enriched melt as temperature cools. In fact, the thermal variations in surface tension $\left(\frac{d\sigma}{dT}\right)$ for the two melts predict that surface tension for the Na–enriched melt is greater by 0.002 N m^{-1} at 850 °C, the temperature of our decompressions. Bagdassarov et al. (2000) also measured surface tension for haplogranitic melt with 20 wt.% Na_2O and found substantially higher surface tensions at 800–900 °C, supporting the conclusion that increased Na_2O contents increases surface tension at temperatures equal to our decompressions. It should be noted that the predicted increase of 0.002 N m^{-1} at 850 °C results from a difference of 5 wt.% Na_2O, which is more than double the difference between our melts (Table 1). We conclude that the ~2 wt.% difference in Na_2O contents of our melts had at best no effect on surface tension, or could have even increased surface tension. Either way, the added Na_2O would not promote bubble nucleation in the F-enriched melts.

Finally, there are small differences in the initial H_2O content between the starting melt compositions (Table 1). We included those in the modeling, but we note that they cannot account for the changes in nucleation. For example, G–1629 (F–03) contained the same amount of dissolved H_2O as G–1609 and G–1645, which both lack added F, and yet G-1629 nucleated orders of magnitude more bubbles at the same value of ΔP (Fig. 2).

5.3. Impact of fluorine on bubble nucleation

The relationships between ΔP and N_B for both suites of experiments show that samples with greater concentrations of F produce higher values of N_B (by up to 3 orders of magnitude) at similar values of ΔP and nucleation time (Fig. 2). We conclude that the increased amount of dissolved F facilitated bubble nucleation and, hence, shortened the induction time. To examine this, we calculate N_B by integrating the equation for nucleation rate, together with mass and momentum balance of the growing bubbles (Toramaru, 1995). Nucleation rate and bubble growth are coupled through pressure and the concentration of dissolved H_2O. The nucleation rate (J) is based on classical nucleation theory and given by

$$J = J_o \exp\left(\frac{-16\pi\sigma^3}{3kT\Delta P^2}\right) \quad (1)$$

where k is the Boltzmann constant, σ is surface tension, and T is temperature. It is assumed that surface tension is constant, whereas ΔP changes over time as a consequence of a change in pressure and in the averaged concentration of dissolved H_2O. The pre-exponential term, J_o, is given by

$$J_o = \frac{n_o^2 V_m D_{H_2O}}{a_o}\left(\frac{\sigma}{kT}\right)^{\frac{1}{2}} \quad (2)$$

where n_o is the concentration of dissolved H_2O molecules, V_m is the molecular volume of H_2O in the melt, D_{H_2O} is diffusivity of molecular H_2O and depends on H_2O concentration, and a_o is the distance between two H_2O molecules in the melt (Hurwitz and Navon, 1994; Navon and Lyakhovsky, 1998). Navon and Lyakhovsky (1998) showed that J_o must change many orders of magnitude in order to substantially change nucleation kinetics. Because the change in N_B between F-poor and F-rich experiments is several orders of magnitude, it is not feasible that the pre-exponential term J_o resulted in the observed differences in nucleation rate and, hence, N_B. Furthermore, because [H_2O] is very similar in all experiments, variations in n_o or a_o are negligible. The only other non-constant parameter in J_o is D_{H_2O}. Although there are no studies that have investigated the impact of [F] on D_{H_2O}, it is reasonable to assume that diffusivity may be affected by F. Changes in D_{H_2O} can also affect the rate at which supersaturation decreases as a result of H_2O diffusion into nucleated bubbles. We therefore assessed the sensitivity of model predictions to the uncertainty in D_{H_2O} by systematically decreasing and increasing D_{H_2O} by one order of magnitude about the value calculated using Zhang and Behrens (2000). We find that our predictions of surface tension are largely insensitive to changes in D_{H_2O} (Fig. 3), supporting our hypothesis that the observed increase in nucleation rate (decrease in induction time) is a consequence of a decrease in surface tension resulting from added F.

Dissolved fluorine is known to decrease melt viscosity (Dingwell et al., 1985; Giordano et al., 2004), and it has been proposed that lower viscosity leads to faster rates of bubble nucleation (Blander and Katz, 1975). Our modeling of bubble nucleation and growth incorporates the influence of F on viscosity of the experimental melts, by using the model of Giordano et al. (2008), which includes the effect of F. We find that the slight changes in viscosity that result from the differences in melt composition have minimal impact on predicted N_B.

We thus find that the difference in N_B between F-rich and F-poor melts is consistent with a decrease in surface

tension (Fig. 3). To examine this further, we focus on samples G–1609 versus G–1613, because they experienced the same decompression conditions, but yet nucleated very different numbers of bubbles (Table 2). We find that the predicted value of surface tension for G–1613, with added F, is $\approx 0.068\ N\ m^{-1}$, and that for G–1609, with little F, is $\approx 0.071\ N\ m^{-1}$; although small, the difference is large enough to make a substantial difference in N_B (Fig. 3). Overall, we conclude that the addition of F decreases surface tension between the exsolving aqueous volatile phase and the surrounding rhyolitic melt by ≈4% (Fig. 3).

5.4. Implications for magmatic degassing

Magmas typically contain 100's to 1000's of ppm F (Carroll and Webster, 1994; Aiuppa et al., 2009). We found that addition of ≤1 wt.% F lowers surface tension of hydrous rhyolite melt by approximately 4% (Fig. 3). Even small decreases in surface tension, however, lower the surface energy of a bubble nucleus and can thus produce substantial increases in bubble nucleation rate (Hurwitz and Navon, 1994). Our results thus indicate that small differences in F content may lead to substantial differences in bubble nucleation kinetics during eruptions.

Surface tension of hydrous silicate melts is also impacted by temperature and melt composition (Bagdassarov et al., 2000; Gardner and Ketcham, 2011; Gardner et al., 2013). Surface tension increases with T by $\sim 6.9 \times 10^{-5}\ N\ m^{-1}\ C^{-1}$. Thus, to reduce surface tension as much as ~1 wt.% F (for rhyolite with ≈6.4 wt.% H_2O), T would have to decrease by ~400 °C. In addition, a range of SiO_2 content from ~50 to 77 wt.% resulted in surface tension for hydrous silicate melts differing by <6%, or little more than the influence of ~1 wt.% dissolved F. We found that the impact that dissolved F has on surface tension is in the same direction as that of added H_2O (Bagdassarov et al., 2000; Gardner et al., 2013). In addition, H_2O and F have similar effects on melt properties and rheology (e.g., Dingwell et al., 1985; Baker and Vaillancourt, 1995; Giordano et al., 2004; Baasner et al., 2013). Although we do not know why dissolved F lowers surface tension, a viable hypothesis is that F dissolves into the melt by breaking bridging oxygen bonds, similar to H_2O (Mysen et al., 2004; Aiuppa et al., 2009). In particular, Mysen et al. (2004) found that F dissolves into highly polymerized aluminosilicate melts, like that used in this study, by forming different types of Na– and Al–bearing fluoride complexes. The dissolution of F results in the depolymerization silicate melt (Mysen et al., 2004; Zimova and Webb, 2007). The effect of dissolved F on melt viscosity differs with melt composition, with the viscosity of melts that are depolymerized by other components showing little effect from added fluorine (Dingwell, 1989; Baasner et al., 2013). The solution mechanisms for fluorine in silicate melts thus depends on melt composition (Carroll and Webster, 1994). This suggests that dissolved fluorine in depolymerized melts would have less of an effect on surface tension, and thus on bubble nucleation.

Our results indicate that F–rich magmas nucleate bubbles at high rates and lower values of ΔP compared to F–poor magmas. Some topaz and tin rhyolites, as well as highly differentiated granitic plutons, contained >5–7 wt.% F (Webster and Duffield, 1994; Webster et al., 2004; Thomas et al., 2005; Webster and Thomas, 2006). Over a wide range of magmatic pressures, F partitioning between melt and most granitic minerals will concentrate F in the melt during magma crystallization and differentiation. Given that an increase in F of ~1 wt.% reduces surface tension by 4%, increasing F in the residual melt to 5–7 wt.% would probably greatly reduce surface tension. It is thus likely that highly F–enriched magmas can nucleate greater numbers of bubbles at lower degrees of supersaturation.

ACKNOWLEDGEMENTS

This work was supported by the National Science Foundation [grant numbers EAR-1348050, EAR-1348072]. We thank two anonymous reviewers for their insight comments, which have strengthened the manuscript.

REFERENCES

Aiuppa A., Baker D. R. and Webster J. D. (2009) Halogens in volcanic systems. *Chem. Geol.* **263**, 1–18.

Baasner A., Schmidt B. C. and Webb S. L. (2013) Compositional dependence of the rheology of halogen (F, Cl) bearing aluminosilicate melts. *Chem. Geol.* **346**, 172–183.

Bagdassarov N., Dorfman A. and Dingwell D. B. (2000) Effect of alkalis, phosphorus, and water on the surface tension of haplogranite melt. *Am. Mineral.* **85**, 33–40.

Baker D. R. and Vaillancourt J. (1995) The low viscosities of F +H_2O-bearing granitic melts and implications for melt extraction and transport. *Earth Planet. Sci. Lett.* **132**, 199–211.

Blander M. and Katz J. L. (1975) Bubble nucleation in liquids. *Am. Inst. Chem. Eng. J.* **21**, 833–848.

Carroll M. R. and Webster J. D. (1994) Solubilities of sulfur, noble gases, nitrogen, chlorine, and fluorine in magmas. *Rev. Mineral. Geochem.* **30**, 231–279.

Dingwell D. B. (1989) Effect of fluorine on the viscosity of diopside liquid. *Am. Mineral.* **74**, 333–338.

Dingwell D. B., Scarfe C. M. and Cronin D. J. (1985) The effect of fluorine on viscosities in the system Na_2O–Al_2O_3–SiO_2: implications for phonolites, trachytes and rhyolites. *Am. Mineral.* **70**, 80–87.

Dobsan P. F., Epstein S. and Stolper E. M. (1990) Hydrogen isotope fractionation between coexisting vapor and silicate glasses and melts at low pressure. *Geochim. Cosmochim. Acta.* **53**, 2723–2730.

Dolejš D. and Baker D. R. (2007) Liquidus equilibria in the system K_2O–Na_2O–Al_2O_3–SiO_2–F_2O_{-1}–H_2O to 100 MPa: I. Silicate-fluoride liquid immiscibility in anhydrous systems. *J. Petrol.* **48**, 785–806.

Donovan J. J. (1995) PROBE: PC-based data acquisition and processing for electron microprobes. Adv. Microbeam 4217.

Gardner J. E. (2009) The impact of pre-existing gas on the ascent of explosively erupted magma. *Bull. Volcanol.* **71**, 835–844.

Gardner J. E. and Ketcham R. A. (2011) Bubble nucleation in rhyolite and dacite melts: temperature dependence of surface tension. *Contrib. Mineral. Petrol.* **162**, 315–331.

Gardner J. E. and Webster J. D. (2016) The impact of dissolved CO_2 on bubble nucleation in water-poor rhyolite melts. *Chem. Geol.* **420**, 180–185.

Gardner J. E., Hilton M. and Carroll M. R. (1999) Experimental constraints on degassing of magma: Isothermal bubble growth during continuous decompression from high pressure. *Earth Planet. Sci. Lett.* **168**, 201–218.

Gardner J. E., Ketcham R. A. and Moore G. (2013) Surface tension of hydrous silicate melts: constraints on the impact of melt composition. *J. Volcanol. Geotherm. Res.* **267**, 68–74.

Giordano D., Romano C., Dingwell D. B., Poe B. and Behrens H. (2004) The combined effects of water and fluorine on the viscosity of silicic magmas. *Geochim. Cosmochim. Acta* **68**, 5159–5168.

Giordano D., Russell J. K. and Dingwell D. B. (2008) Viscosity of magmatic liquids. A model. *Earth Planet Sci. Lett.*. https://doi.org/10.1016/j.epsl.2008.03.038.

Gonnermann H. M. and Gardner J. E. (2013) Homogeneous bubble nucleation in rhyolitic melt: experiments and nonclassical theory. *Geochem. Geophys. Geosys.* **14**, 4758–4773.

Holtz F., Dingwell D. B. and Behrens H. (1993) Effects of F, B_2O_3, and P_2O_5 on the solubility of water in haplogranitie melts compared to natural silicate melts. *Contrib. Mineral. Petrol.* **113**, 492–501.

Holtz F., Behrens H., Dingwell D. B. and Johannes W. (1995) H2O solubility in haplogranitic melts: compositional, pressure, and temperature dependence. *Am. Mineral.* **80**, 94–108.

Hurwitz S. and Navon O. (1994) Bubble nucleation in rhyolitic melts: experiments at high pressure, temperature, and water content. *Earth Planet. Sci. Lett.* **122**, 267–280.

Kashchiev D. (2000) *Nucleation: Basic Theory with Applications*. Butterworth-Heinemann, Oxford, U.K..

Kiprianov A. A. (2006) Regular trends in uptake of halogens by alkali silicate glasses containing two glass-forming components. *Russ. J. App. Chem.* **79**, 20–28.

Liu Y., Zhang Y. and Behrens H. (2005) Solubility of H_2O in rhyolitic melts at low pressure and a new empirical model for mixed H_2O-CO_2 solubility in rhyolitic melts. *J. Volcanol. Geotherm. Res.* **143**, 219–235.

Mangan M. T. and Sisson T. W. (2000) Delayed, disequilibrium degassing in rhyolite magma: decompression experiments and implications for explosive volcanism. *Earth Planet. Sci. Lett.* **183**, 441–455.

Manning D. A. C. (1981) The effect of fluorine on liquidus phase relationships in the system Qz–Ab–Or with excess water at 1 kb. *Contrib. Mineral. Petrol.* **76**, 206–215.

McIntosh I. M., Llewellin E. W., Humphreys M. C. S., Nichols A. R. L., Burgisser A., Schipper C. I. and Larsen J. F. (2014) Distribution of dissolved water in magmatic glass records growth and resorption of bubbles. *Earth Planet. Sci. Lett.* **401**, 1–11.

Mourtada-Bonnefoi C. C. and Laporte D. (1999) Experimental study of homogeneous bubble nucleation in rhyolitic magmas. *Geophys. Res. Lett.* **26**, 3505–3508.

Mysen B. O., Cody G. D. and Smith A. (2004) Solubility mechanisms of fluorine in peralkaline and meta-aluminous silicate glasses and in melts to magmatic temperatures. *Geochim. Cosmochim. Acta* **68**, 2745–2769.

Navon O. and Lyakhovsky V. (1998) *Vesiculation processes in silicic magmas*. Geol. Soc. Lond. Spec. Pub, pp. 27–50.

Shartsis L. and Spinner S. (1951) Surface tension of molten alkali silicates. *J. Res. Nat. Bur. Stand.* **46**, 385–390.

Sparks R. S. J. (1978) The dynamics of bubble formation and growth in magmas: a review and analysis. *J. Volcanol. Geotherm. Res.* **3**, 1–37.

Thomas R., Förster H.-J., Rickers K. and Webster J. D. (2005) Formation of extremely F-rich hydrous melt fractions and hydrothermal fluids during differentiation of highly evolved tin-granite magmas: a complex melt/fluid-inclusion study. *Mineral. Deposita* **148**, 582–601.

Toramaru A. (1995) Numerical study of nucleation and growth of bubbles in viscous magmas. *J. Geophys. Res.* **100**, 1913–1931.

Webster J. D. and Duffield W. A. (1994) Extreme halogen abundances in tin-rich magma of the Taylor Creek rhyolite, New Mexico. *Econ. Geol.* **89**, 840–850.

Webster J. D. and Thomas R. (2006) *Silicate melt inclusions in felsic plutons: a synthesis and review*. Min. Assoc., Canada, pp. 165–188.

Webster J. D., Thomas R., Förster H.-J., Seltmann R. and Tappen C. (2004) Geochemical evolution of halogen-enriched, granite magmas and mineralizing fluids of the Zinnwald tin-tungsten mining district, Erzgebirge, Germany. *Mineral. Depos.* **39**, 452–472.

Zhang Y. and Behrens H. (2000) H_2O diffusion in rhyolitic melts and glasses. *Chem. Geol.* **169**, 243–262.

Zhang Y., Belcher R., Ihinger P. D., Wang L., Xu Z. and Newman S. (1997) New calibration of infrared measurement of dissolved water in rhyolitic glasses. *Geochim. Cosmochim. Acta* **61**, 3089–3100.

Zimova M. and Webb S. L. (2007) The combined effects of chlorine and fluorine on the viscosity of aluminosilicate melts. *Geochim. Cosmochim. Acta* **71**, 1553–1562.

Associate editor: Wim van Westrenen